Available online at www.sciencedirect.com
ScienceDirect
Journal of Magnetic Resonance 187 (2007) 10–18
JMR Journal of Magnetic Resonance
www.elsevier.com/locate/jmr

# A novel low-E field coil to minimize heating of biological samples in solid-state multinuclear NMR experiments

Baudouin Dillmann [a], Karim Elbayed [b,*], Heinz Zeiger [a], Marie-Catherine Weingertner [b], Martial Piotto [c], Frank Engelke [a]

[a] Bruker Biospin GmbH, Silberstreifen, D-76287 Rheinstetten, Germany
[b] Universite Louis Pasteur/CNRS LC3-UMR7177, Institut/Faculte de Chimie, 4, rue Blaise Pascal, F-67070 Strasbourg, France
[c] Bruker Biospin, 34 rue de l'Industrie, F-67166 Wissembourg, France

Received 18 October 2006; revised 20 February 2007
Available online 31 March 2007

**Abstract**

A novel coil, called Z coil, is presented. Its function is to reduce the strong thermal effects produced by rf heating at high frequencies. The results obtained at 500 MHz in a 50 μl sample prove that the Z coil can cope with salt concentrations that are one order of magnitude higher than in traditional solenoidal coils. The evaluation of the rf field is performed by numerical analysis based on first principles and by carrying out rf field measurements. Reduction of rf heating is probed with a DMPC/DHPC membrane prepared in buffers of increasing salt concentrations. The intricate correlation that exists between the magnetic and electric field is presented. It is demonstrated that, in a multiply tuned traditional MAS coil, the rf electric field $E_1$ cannot be reduced without altering the rf magnetic field. Since the detailed distribution differs when changing the coil geometry, a comparison involving the following three distinct designs is discussed: (1) a regular coil of 5.5 turns, (2) a variable pitch coil with the same number of turns, (3) the new Z coil structure. For each of these coils loaded with samples of different salt concentrations, the nutation fields obtained at a certain power level provide a basis to discuss the impact of the dielectric and conductive losses on the rf efficiency.


*Keywords:* NMR coils; $E_1$ Field; $B_1$ Field; Rf heating; Bicelles; Dielectric dispersion; Electromagnetic numerical modeling

## 1. Introduction

The reduction of radiofrequency (rf) heating in biologically relevant NMR samples has become a major challenge for the design of novel coils in NMR probes [1–4]. The principal mechanisms that lead to rf heating in NMR samples have been known for decades [5,6]. In NMR the impact on lossy samples of the rf electric field ($E_1$ field), which is always present along with the rf magnetic field ($B_1$ field), is particularly noticeable at high frequencies. The dispersion of the NMR sample arises from two sources: the most remarkable one is related to the imaginary part of the dielectric permittivity for a certain frequency range and the second one is linked to the electric conductivity [7–10]. A dispersive sample represents a lossy element in the rf circuit of the NMR probe and leads to a strong decrease of the resonance frequency of the tuned rf circuit. Such phenomenon is caused by the increase of the equivalent coil-to-sample capacitance [6]. This is particularly noticeable for the high-frequency channel of the probe, usually tuned to the $^1$H frequency. As a result the tuning range has to be enlarged in order to compensate for samples with a high dielectric dispersion.

If lossy samples are brought into a given electromagnetic field, the latter is changed [9], i.e., the field distribution becomes different from the one in air or vacuum or from the one in a low loss sample. Losses originating from the dielectric or conductive properties of the sample lead to energy dissipation. The effective current induced in

* Corresponding author. Fax: +33 3 88 415359.
*E-mail address:* elbayed@chimie.u-strasbg.fr (K. Elbayed).

1090-7807/$ - see front matter © 2007 Elsevier Inc. All rights reserved.
doi:10.1016/j.jmr.2007.02.018

conductive samples [8,9,11] couples with the $E_1$ field and dissipation leads to heating. This may result in unwanted phase transitions of the sample due to the internal temperature change and, in some extreme cases, the degradation or the destruction of the sample may happen. Finally, sample losses also change the impedance matching between the input ports of the NMR probe and the preamplifiers connected by 50 Ω cables and they lower the Q factor of the probe circuit hence they affect the signal-to-noise ratio of the NMR experiment [6].

From the viewpoint of NMR probe engineering it is highly desirable to design and construct NMR coils or resonators that allow to minimize rf heating of lossy NMR samples like biological membranes or protein samples. The aim of this work is to present a novel coil structure, called Z coil, which is, as the regular coil, designed for multinuclear experiments in a solid-state NMR probe. The novel Z coil is characterized both electromagnetically as well as from the NMR experiment point of view. In general, NMR coils need to satisfy simultaneously the following requirements: (i) to produce a maximum rf magnetic field at the coil and sample center, (ii) to minimize the rf electric field components inside the volume occupied by the sample, hence to minimize the electric field energy and therefore dissipation inside the sample, (iii) to provide a high homogeneity of the rf magnetic field over the sample volume. The rf electric and magnetic field components are not independent of each other. They are linked via Maxwell's equations. The coil or resonator geometry, the surrounding rf circuit, and the sample geometry (i.e., the sample location and distribution inside the coil), represent boundary conditions, under which Maxwell's equations are to be solved. A detailed analysis shows, that for many cases minimizing the $E_1$ field and homogenizing the $B_1$ field by adapting the geometry of the coil comes at the expense of $B_1$ field amplitude in the center of the coil. Based on the standard solenoidal or helix coil used in solid-state NMR probes, described extensively in [10], serious attempts have been made to improve the homogeneity, e.g. by varying the pitch [12], or using variable-width wire [13]. On one side the novel Z coil structure to be introduced in this paper is a continuation of this art of modifying solenoidal coils by introducing spiral coils to localize the $E_1$ field in a radial plane [3,14] outside the center of the sample and coil. On the other side, the '$E_1$ field relocating' spiral coils are connected with a central loop that provide a homogeneous $B_1$ field within the sample. In the present paper we will show some of the interesting features of Z coils in comparison with the classical solenoidal coils by investigating in more detail the electromagnetic field distribution of the Z coil by calculation and by experiment. The rf heating effects caused on bicelle samples will be measured as a function of salt concentration in the sample.

## 2. Temperature monitoring in bicelle samples

Quantitation of sample heating in NMR experiments requires measurement of the sample temperature *in situ*. NMR thermometers based on temperature dependence of the chemical shift are available to calibrate the temperature inside the sample. For $^1$H NMR spectroscopy one of the most popular methods is to use methanol or ethylenglycol, whose OH and $CH_2$ peaks [15] experience a well known temperature dependence of the frequency shift. Compounds containing lanthanides like TmDOTP5 (thulium 1,4,7,10-tetraazacyclododecane-1,4,7,10-tetrakis(methylene phosphonate)) also have been successfully used to measure temperature via the $^1$H chemical shift [3]. Other NMR nuclei contained in temperature sensitive materials are $^{13}$C, $^{19}$F, and $^{59}$Co [16] for liquids, and $^{207}$Pb [17] for solids. For lipid membranes the addition of reference compounds may interact with the sample and in practice the best method is to use the water [4] in most biological samples.

Bicelle samples like DMPC/DHPC assemblies are membrane models which require a very careful temperature handling [18,19]. $^2$H NMR allows us to investigate the exchange of water from the bath to the bound state. The splitting of deuterium (spin 1) resonance lines originating from the coupling of the quadrupolar moment with the local electric field gradient (arising from neighboring atoms or molecules) has been investigated in the so called swelling regime where the hydration plays a major role [20,21]. There exists a region of temperatures between 298 and 317 K, where the bicelles form a homogeneous phase, and the quadrupolar splitting of $^2$H in $D_2O$ is governed by the order parameter of the system. In this temperature range the quadrupolar splitting increases linearly with temperature. The phase diagram is rather insensitive to variations of the salt concentration [22] and the same model can be applied to monitor the temperature increase.

## 3. Z coil geometry

The main mechanical elements and the overall geometry of the here presented Z coil are shown in Fig. 1. The Z coil consists of a copper cylinder with a helical slit. The resulting 1.5 mm wide gap carries out a 180° turn from one end to the other end of the resonator. We refer to the cylindrical part as the *core* of the Z coil. At the two extremities, two spirally wound and flattened wires are connected. On the outer turns these *spiral coils* (Archimedes spirals, 3 turns, inner diameter 4.5 mm, outer diameter 9 mm) are

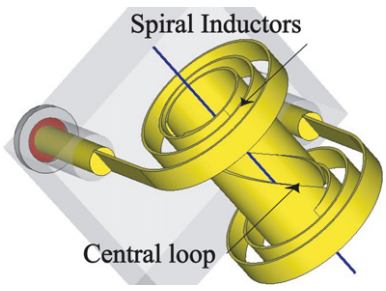


Fig. 1. Z coil resonator with the two main construction elements: the spiral coils at opposite ends of the resonator and the central loop.

soldered to the coil leads at opposite corners of the ceramic block that serves as the coil holder [23]. The Z coil resonator is the central part of an rf circuit that provides an electrically balanced voltage distribution between the two coil leads for one, two, or even three different frequencies. An example of such a circuit can be found in [24].

It is the complete structure, depicted in Fig. 1, including the two spiral coils and the central core embedded in the coil holder, that defines the self-resonance frequency. The latter can be measured, for example, using a pickup coil connected through a 50 Ω cable to the network analyzer. The geometric dimensions of the Z coil are chosen in such a way that the self-resonance frequency stays above the desired proton resonance frequency (here, 630 MHz to be used in a 500 MHz rf circuit). Therefore the Z coil appears as an inductive element in a multi-channel circuit, e.g., for a probe tuned to $^{1}$H and to $^{13}$C, $^{15}$N or $^{2}$H. In contrast to a loop-gap resonator [25,26] the Z coil is easily tunable to multiple frequencies. As such, it is similar to a solenoid coil, except that the self-resonant mode of the solenoid contains much more electric field inside the coil than the Z coil. Unfortunately, away from its self-resonance frequency the Z coil will exhibit less magnetic field than a regular coil, as is expected for such low-E structures [3,26,27]. However, as shown further below in the present paper, for lossy samples this apparent drawback will turn out as not significant: for lossy samples the rf efficiency of the Z coil and the solenoidal coil almost coincide.

## 4. Rf field mapping

### 4.1. Electromagnetic field simulation

We have applied computational techniques for electromagnetic fields based on first principles to evaluate the spatial distribution of the high-frequency $E_1$ and $B_1$ field characteristics for the Z coil. One goal was to prove by simulation that coil geometries can be found where the $E_1$ field is distributed in such a way that it is minimum or negligibly small within the sample volume. Since our problem at hand has a fairly complex spatial arrangement, it was ruled out from the beginning to attempt to solve Maxwell's equations by analytical techniques. Therefore we decided to employ numerical methods based on discrete models. The Finite Integration Technique (FIT) proposed and developed by Weiland [28,29] and implemented in the software program Microwave-Studio® (MWS 2006) by Computer Simulation Technologies, Darmstadt (CST) has been applied to find the electromagnetic field distribution of the Z coil.

The relevance of this technique has already been demonstrated in the literature for the study of NMR coils [9,27]. The numerical simulation was based on the Z coil structure depicted in Fig. 1. A display of the magnetic vector field in an axial plane OYZ is shown in Fig. 2. This magnetic field distribution results from the analysis using the transient solver module of MWS applied to a Z coil loaded with a sample consisting of a 18 mm long tube made of $ZrO_2$ ceramics ($\varepsilon_r \approx 30$) of outer diameter 4 mm, inner diameter 3 mm, filled with a 5 mm long sample of salty water (conductivity 2 S/m) at the center of the coil. The relative permittivity $\varepsilon_r$ of this solvent has a complex value whose real part is equal to 81 and whose imaginary part is equal to 72 at a frequency of 500 MHz, leading to some energy dissipation. The two excitation ports (in Fig. 2 surrounded by red squares) are fed with excitation pulses, 180° out of phase from each other to simulate external circuit balance.

It is interesting to note that the maximum of the magnetic field is located outside of the sample, close to the conducting wall of the Z coil core. Nevertheless, the amplitude value of the field in the center of the sample is relatively high, although lower than the amplitude close to the core walls. Moreover, its distribution inside the core is highly homogeneous. Therefore it leads to the highest density that would be encountered in the field histogram of the $B_1$ field [30,31]. For the Z coil and for the variable pitch coil the field profiles shown in Fig. 3a correspond to the vector component of $B_1$ along the coil axis, while the distributions in Fig. 3b display the $E_1$ field magnitude. For both distributions shown in Fig. 3, a nonconductive sample has been assumed where the losses originate from dielectric dispersion only. The dispersion behavior in the simulation was based on a Debye model with a dielectric relaxation time of $4.6 \times 10^{-10}$ s. According to Gimsa [8], this large value is characteristic for bound water on lipid headgroups of membranes. It is about 200 times larger than the relaxation time constant for nonbound water molecules (ca. $9 \times 10^{-12}$ s).

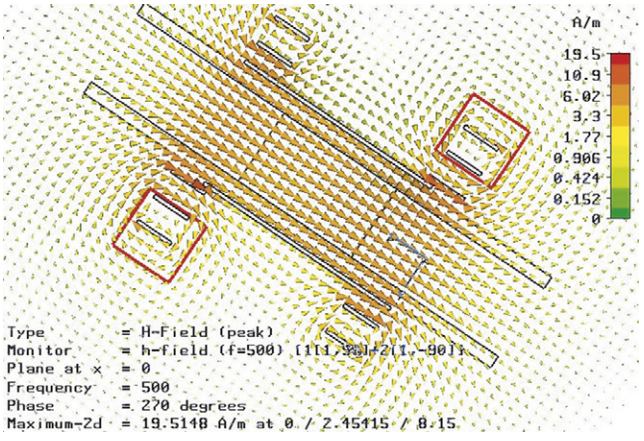


Fig. 2. Axial plane cross section of the sample-loaded Z coil for rf field simulations. The magnetic vector field distribution is indicated by small triangles. All simulations were performed with the CST software Microwave Studio (CST-MWS) transient solver. Gaussian shaped pulses were applied at both terminal ports (red squares) of the coil with opposite electric phase (to simulate a balanced circuit) at 500 MHz. A 5 mm long conductive water sample was positioned in a dielectric cylinder of 18 mm length to evaluate the impact of the complex permittivity of conductive samples. (For interpretation of the references to color in this figure legend, the reader is referred to the web version of this paper.)

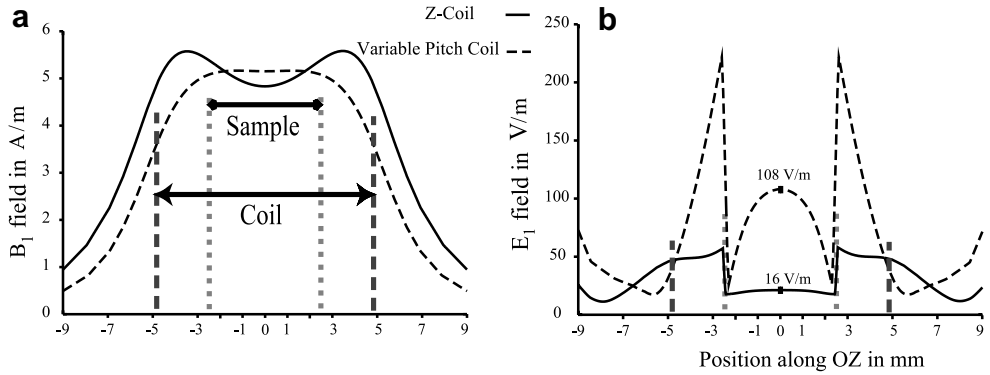


Fig. 3. $B_1$ and $E_1$ field profiles along the axis of the loaded Z coil. The abscissa corresponds to a length of 18 mm. The vertical dotted lines indicate the extension of the coil and of the water sample in the Z coil. The ordinate axis of (a) shows the rf magnetic field magnitude $B_1$ along the coil axis. The horizontal line indicates the inhomogeneity in the maximum field region. The ordinate axis of (b) measures the electric field magnitude $E_1$.

It is useful to consider the ratio $E_1/B_1$ at a given point in space for comparing simulated fields in different coils. For the Z coil, $E_1/B_1$ is computed to be approximately equal to 3.2 V/A in the center of the dispersive sample, while it reaches 21.0 V/A in the center of a variable-pitch coil (applying the same boundary conditions). The $E_1$ field magnitude distribution in a plane containing the center of the core is plotted in Fig. 4. The plane for this contour plot coincides with the plane for the $B_1$ field distribution in Fig. 2. We point out that the $E_1$ field is concentrated in the spirals and decreases when coming closer to the core. We found furthermore by additional simulations, that the size of the gap has almost no influence on the self-resonance frequency of this coil. In practice, most of the $E_1$ field is stored in the spiral coils and not in the helical gap of the core. The latter would be the case for the self-resonant mode of the loop-gap resonator.

However, the gap width plays a role for the distribution of the radial $B_1$ field component, as it does in a loop-gap resonator [25] or in a scroll coil [27]. Recently, it has been shown [32] for the case of solenoidal coils that the inhomogeneous distribution of the radial component of the $B_1$ field leads to modulation effects in experiments performed under sample spinning conditions (e.g., MAS). In order to estimate the amplitude of the radial component of the $B_1$ field in the Z coil, we performed simulations to compare the variation of the radial component of $B_1$ along a circular path of 1 mm radius for a single-turn coil (loop of 4.2 mm radius, wire thickness 0.5 mm) with the radial field variation along the same path in a Z coil (4.2 mm radius, gap width 0.5 mm). For the single-turn loop the variation of the radial $B_1$ component amounts to about 10% of the axial $B_1$ component value at the loop center, for the Z coil this variation is only ca. 2%. A similar comparison has been made for the $E_1/B_1$ magnitude ratio. While for the single-turn loop the value of the $E_1/B_1$ ratio at the center is equal to 12.7 V/A, this ratio is as low as 1.9 V/A for the Z coil (Supplementary material).

From the rf circuit perspective, the Z coil behaves very similar to a regular solenoid. Thus, no additional means were necessary to tune or match the rf circuit of the probe. Regarding the $B_1$ and $E_1$ field distributions the Z coil is different from the classical solenoidal coil. The spatial separation of the rf electric and magnetic fields in the Z coil is much more pronounced than in a solenoidal coil [10].

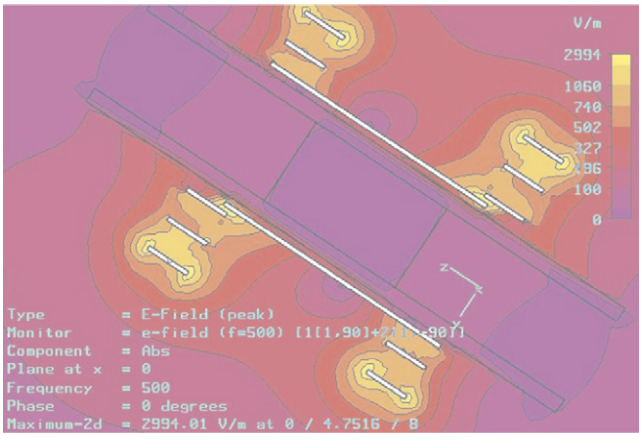


Fig. 4. Axial plane cross section representing the $E_1$ field magnitude in a plane located in the same position as in Fig. 2. The maximum of the $E_1$ field is located at the tip of the spiral coil leads. The minimum of $E_1$ is located inside the core where the water sample is located. The contours are at 17 levels spaced from 0 to 3000 V/m (logarithmic scale).

### 4.2. Experimental determination of $B_1$ field profiles for coils of various geometries

In order to experimentally determine the $B_1$ field distribution inside resonators or coils, small metallic (e.g., spherical) bodies were positioned into the region of interest. The presence of the metallic ball leads to a local perturbation of the $B_1$ field (the interior of the ball is field-free, at the surface the external rf field induces currents that generate additional fields superimposed to the external rf field). In terms of circuit parameters like the inductance of the coil, the positioning of the ball inside the coil results in a decrease of the apparent inductance value and therefore in an increase $\Delta f_{bs}$ of the resonance frequency of the tuned

and matched circuit. Such so-called "*ball shift*" measurements $\Delta f_{bs}$ provide a mapping [33,34] of the $B_1$ distribution. In other words, the value of the frequency shift for a given position of the metallic ball is a (monotonous) function of the $B_1$ field amplitude at the same location. We have used a set of Kel-F inserts containing an embedded copper ball (diameter 3 mm) to probe the field by positioning these inserts along the main axis of the coils (of length 9 mm and diameter 4.2 mm and for the solenoid with 5.5 turns and the same length and diameter) with incremental steps of 0.5 mm. The three profiles measured at a frequency of 500 MHz shown in Fig. 5 were taken for a regular and variable-pitch solenoidal coil as well as for the Z coil.

As it becomes clear from Fig. 5, the solenoidal coil with a variable pitch has a higher $B_1$ homogeneity than the regular solenoid [12,35], but also a slightly decreased maximum value. The improved homogeneous plateau of the Z coil exhibits simultaneously a slight decrease of the maximum value of the ball shift in the coil center when compared to the regular solenoidal coil. The results of the profile measurement obtained for the Z coil are in agreement with the calculated magnetic field profile shown in Fig. 3. The ball shift *per se* can be related only indirectly to the $B_1$ field. The portion of the magnetic field energy stored in the volume equal to the ball volume (when the ball is absent) may serve to define the magnetic filling factor [33] :

$$\xi_{bs} = 1 - \left(\frac{f_1}{f_1 + \Delta f_{bs}}\right)^2 \tag{1}$$

where $f_1$ denotes the circuit resonance frequency measured with an empty insert. If we want to compare different coils, it is the magnetic filling factor that turns out to be relevant to relate $B_1$ field magnitudes to each other at a given position inside the respective coil. In our particular case the magnetic filling factor, measured by the ball shift at the respective coil centers, is almost equal for the variable pitch and the regular coil, $\xi_{bs} \approx 0.0175$. It is smaller for the Z coil, where we obtain $\xi_{bs} \approx 0.0056$. From the fact that the magnetic energy density $B_1^2/2\mu_0$ is equal to the rf power $P^e$ supplied to the probe, multiplied by the magnetic filling factor $\xi_{bs}$ divided by the frequency bandwidth $\omega_0/Q_l$ of the probe and divided by the volume of the element referring to $\xi_{bs}$ , the expression for the field magnitude $B_1$ as a function of the filling factor $\xi_{bs}$ is given by

$$B_1 = k\sqrt{\frac{2\mu_0 P^e \xi_{bs} Q_l}{\omega_0 V}} \tag{2}$$

where $Q_l$ denotes the quality factor of the circuit with the lossy sample inside the rf coil, and $\omega_0$ is equal to the angular rf frequency. The filling factor $\xi_{bs}$ is measured relative to the volume element $V$. The factor $k$ takes into account the orientation of the coil or resonator axis relative to the external static field $B_0$ . From this equation it is noticeable that $B_1$ measured in an NMR nutation experiment will increase linearly with the square root of the power supplied to the probe as it will be shown below in Fig. 8 for $^1$H and $^2$H nuclei.

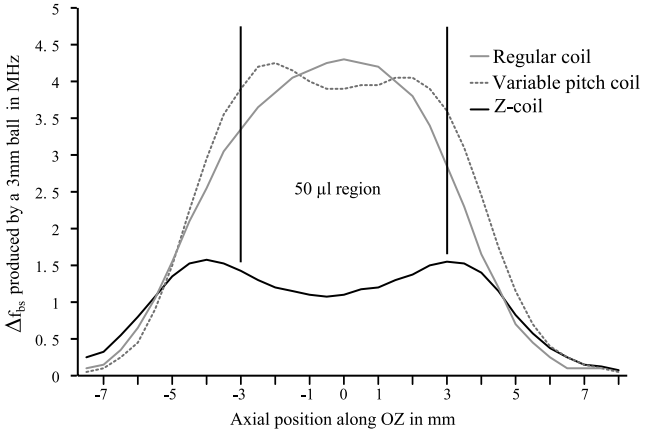


Fig. 5. Rf magnetic field profile at 500 MHz for various 4 mm inner diameter coils (regular solenoid, variable-pitch solenoid, and Z coil) obtained by ball-shift measurements. The frequency shift $\Delta f_{bs}$ caused by the metal ball in the insert as measured by connecting an Agilent 8712ET network analyzer to the matched probe and recording the frequency of the wobble curve minimum. The frequency shift was taken relative to the frequency of the wobble curve minimum of an insert without ball.

## 5. NMR experiments to measure rf heating in bicelle samples

In order to verify the practical consequences of the $E_1$ field distribution in the solenoidal coils and the Z coil, we have performed NMR experiments on bicelle samples. All experiments were performed on a Bruker AVANCE spectrometer equipped with a 500 MHz widebore magnet. The rf power at the probe input ports was measured with an oscilloscope Agilent DS06102A using a 30 dB attenuator. The NMR probe comprised a double resonance circuit with the $^1$H channel tuned to 500 MHz and the low frequency channel tunable from 50 to 205 MHz. The probe was equipped with a 4 mm MAS system. The rf heating experiments described below were performed under static conditions. The assembly of the various coils in the probe did not require any modifications of the probe rf circuit—only the variable tuning and matching capacitors had to be adjusted. The Q factor of the NMR probe was measured from the reflection curve for a matched channel by means of a vectorial network analyser Agilent 8712ET.

### 5.1. NMR on bicelles

Bicelles from Avanti Polar Lipids were prepared as described in the literature [20,21,36] at a concentration of 25% w/v (250 mg/ml). As proposed recently [37] the molar ratio $q = 3$ has been chosen for the two lipids DMPC/DHPC. The sample was prepared in a phosphate buffer (pH 6), 10% $D_2O$ was added for the study of $^2$H exchange NMR spectra. The sample conductivity was varied by adding PBS (a mixture of $K_2HPO_4$ and $KH_2PO_4$) to produce

three different salt concentrations of 10, 50 and 100 mM. A reference sample without salt was also investigated. All samples were packed in a (non-spinning) 4 mm rotor and all coils were consecutively assembled in the same double resonance MAS probe. The variation of the NMR line frequency vs. temperature change, $\Delta\nu_{bic}/dT$, measured prior to the start of the following experiments, is equal to 1.2 Hz/K. This value is independent of the salt concentration [22,38]. In order to ensure thermal stability, the gas flow around the sample was maintained (at a pressure of 770 mB, without spinning the sample) using a gas flow cooling unit (BCU-05), while the temperature controller (BVT-2000) was used to control the probe heater by measuring the temperature directly in the gas flow at the MAS stator close to the sample. Once the data were recorded at variable temperatures, these values could be used to monitor the increase in temperature, relative to the value of 305 K, originating from the $E_1$ field of the rf coil. The pulse sequence employed to monitor the heating due to the rf electric field at the $^1$H frequency went as follows : 0.5 s $^1$H rf pulse prior to $^2$H 90° pulse followed by 1 s pulse of $^1$H CW irradiation during the $^2$H FID acquisition to mimic a long decoupling pulse at different $B_1$ field amplitudes in the range from 5 to 16 kHz. These $B_1$ field amplitudes were measured by determining the length of the 360° pulse for $^1$H at different rf power levels for each sample and each coil. The same power level was applied 10 times before the next increment to measure rf heating step by step. The $^2$H NMR spectra presented in Fig. 6 are plotted as a function of the $^1$H $B_1$ field amplitude. A phase transition occurs in the bicelle sample placed in a regular coil, when the $B_1$ amplitude becomes greater than 9.5 kHz. Temperature calibration measurements with the bicelle sample show that the phase transition occurs at about 317 K. Additional sample heating due to spinning [4,39] is avoided in our experiments. Therefore the heating of the sample results solely from the presence of the rf electric field inside the sample. Measuring the temperature increase as a function of the applied field amplitude $B_1$ allows to quantify the impact of the electric field $E_1$ in the coil [4,27]. Such data are shown in Fig. 7 for the three different coils whose $B_1$ field profiles were already compared in Fig. 5.

The data presented in Fig. 7 confirm in a quantitative way that the greater the salt concentration, the higher the rf heating. Furthermore it becomes evident that the Z coil has a much lower $E_1$ field than the two other coils as predicted from the computer simulation (Figs. 3 and 4). The temperature increase in the samples containing up to 100 mM PBS in the Z coil remains comparably low when compared to a regular solenoidal coil with a sample of 10 mM PBS. For the regular and the variable-pitch coil, all salty samples exhibited the phase transition (Fig. 6). Thus, while the replacement of the regular solenoidal coil by a variable-pitch coil is a reasonable choice for the lower salt concentrations, the Z coil appears superior when the sample exhibits higher salt concentrations.

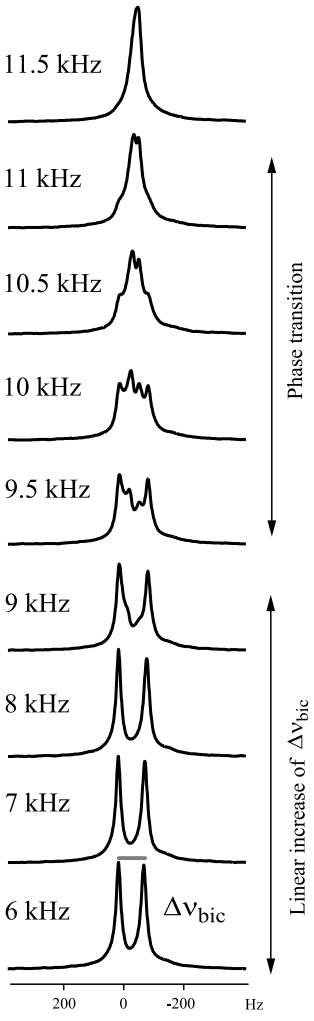


Fig. 6. Series of $^2$H NMR spectra of deuterated water in the DMPC/DHPC system. The quadrupolar splitting (in Hz) appears as a function of the applied $B_1$ field magnitude. The measurements were done at 76.8 MHz ($^2$H), obtained with packed samples (ca. 50 μl) inserted into a regular 4 mm solenoidal coil. All experiments were conducted with non-spinning samples. Alignment of bicelles was obtained after 30 min to 1 hour waiting time, the overall series of experiments took 30–40 min. By increasing the power level of the $^1$H channel, the increasing $E_1$ field leads to heating which in turn modifies the dynamics of water in the samples. The phase transition indicated by the vanishing splitting (upper spectrum) corresponds to a equivalent temperature of 317 K. In an MAS stator whose temperature was stabilized at 305 K, the heating produced by the rf pulse in the $^1$H channel on a 100 mM PBS salt amounts to a temperature increase up to 12 K for $B_1$ field amplitudes in the range from 1 to 12 kHz.

### 5.2. Comparison of NMR nutation fields for regular solenoids and Z coils

Apart from the detailed electromagnetic field distribution of the coils and the quantitative evaluation of rf heating effects, it is important to measure and compare the rf efficiency of the Z coil with that one of a solenoidal coil. For that purpose the NMR nutation field [31] was determined as a function of the rf power supplied at the input port of the $^1$H and the $^2$H probe channels. The data obtained from these experiments are shown in Fig. 8 for

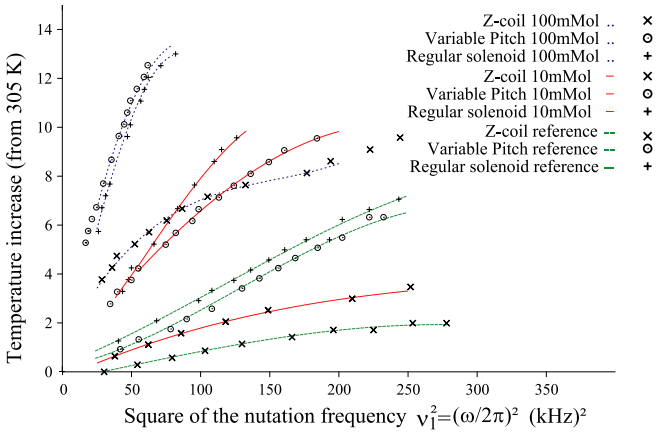


Fig. 7. Sample temperature increase induced by an increasing rf field at 500 MHz ($^1$H resonance frequency) as function of the PBS concentration. The temperature increase was inferred from the $^2$H quadrupolar splitting by using the same linear model for all samples.

the bicelle sample, spinning at the magic angle at a rate of 4 kHz. The abscissa in Fig. 8 represents the square root of rf power, and because each curve passes through the origin and exhibits a linear behavior, only relatively few points are needed to predict the slope of each straight line. In addition to the bicelle sample, nutation rate in deuterated adamantane (same volume as the bicelle sample) spinning at a rate of 4 kHz was measured. The results from the $^2$H probe channel are represented in Fig. 8a, while the data for $^1$H are displayed in Fig. 8b. The slope of each particular line defines the rf efficiency or power conversion factor $\eta$ of the respective channel for the given coil with the specific sample in the coil, measured in units of nutation frequency squared per unit of power (e.g., in kHz$^2$/watt). Focusing first on the data obtained for adamantane which represents a sample with low dielectric and no conductive losses, it becomes evident that in terms of rf efficiency (slope of straight lines in Fig. 8) the solenoidal coil is superior to the Z coil for the $^1$H as well as for the $^2$H channel. The situation becomes different for a bicelle sample which is dielectrically lossy and conductive. The Z coil now meets the solenoidal coil in rf performance. These findings also confirm the results reported in [6,9,40]: at a given power level the nutation frequency, hence the rf field amplitude, depends on the dielectric and conduction properties of the NMR sample inside the NMR coil.

A quantitative analysis of the power conversion factors summarized in Table 1, in analogy of the discussion presented in [1], requires a more thorough definition of the heat deposited in lossy samples. In addition to the definition of power conversion factors (with $\nu_{1nl}$ and $\nu_{1bio}$ denoting the nutation frequencies),

$$\eta_{nl} = \nu_{1nl}^2/P_{nl}, \quad \eta_{bio} = \nu_{1bio}^2/P_{bio} \tag{3}$$

for nonlossy samples (e.g., adamantane) and biological samples (e.g., bicelles) we define the power $P_{heat}$ lost in the biological sample relative to a sample without losses:

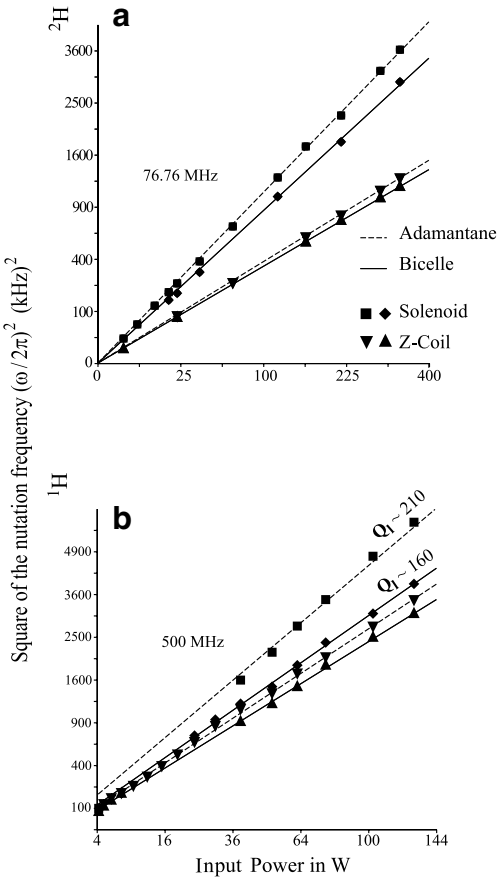


Fig. 8. Measure of the nutation frequency squared per unit of power (a) for the $^2$H channel, (b) for the $^1$H channel. The nutation curves were obtained with deuterated adamantane and bicelles. The quality factor of the $^1$H probe circuit in presence of the sample is indicated for the solenoidal coil for the adamantane (high Q value) and the bicelle sample (lower Q value). For the Z coil the Q factor did not differ for the two samples. All data were taken under MAS at 4 kHz.

Table 1
Power conversion coefficients for the $^1$H channel as defined by the slopes of straight lines in Fig. 8b and heat deposition as defined in Eq. (5)

| | $\eta$ (Adamantane) (kHz$^2$/W) | $\eta$ (Bicelle) (kHz$^2$/W) | $q_{heat}$ (mW/kHz$^2$) |
|---|---|---|---|
| Z coil | 27.0 | 24.0 | 4.7 |
| Solenoid | 44.9 | 30.2 | 10 |

$$P_{heat} = P_{bio} - P_{nl} \tag{4}$$

at the same nutation frequency ($\nu_{1nl} = \nu_{1bio} = \nu_1$). The heat deposition of a biological sample,

$$q_{heat} = \frac{P_{heat}}{\nu_1^2} = \frac{1}{\eta_{bio}} - \frac{1}{\eta_{nl}} \tag{5}$$

characterizes, for one given nutation field $\nu_1$, the power dissipated in the biological sample. Hence, $q_{heat}$ is a meaningful measure to compare coils loaded with lossy samples. From the values of Table 1 we infer that the Z coil deposits two times less heat in the bicelle sample than the solenoidal coil.

## 6. Conclusions

The physical mechanism of water heating by microwaves at a certain frequency is well known. In recent articles the impact of the electromagnetic field on water in lipid bilayers has been addressed [7,8]. Water molecules in a 5 nm layer above the polar headgroups [8] reveal a dielectric relaxation time which is two orders of magnitude longer than the dielectric relaxation time found in free water. This means that dielectric dispersion effects already occur at frequencies as low as 500 MHz. The resulting heat dissipation, leading to a temperature change of hydrated bicelle samples, affects the $D_2O$ exchange on these bicelles and, as demonstrated by the results in the present paper, this $D_2O$ exchange process is a suitable means to monitor the temperature increase of the sample.

In nondispersive samples, because the Z coil has an rf efficiency lower than the regular solenoidal coil, the intensity of the NMR signal for $^1H$ as well as for $^2H$ is smaller in the Z coil as compared to the solenoid. On the other hand, the experimental results of rf heating (Fig. 7) for lossy samples demonstrate that the ratio $B_1/E_1$ for the interior of the Z coil is significantly higher than for the solenoidal coil—mainly because $E_1$ is so small inside the Z coil. Therefore, for samples with high dielectric dispersion and/or electric conductivity we conclude from the data of Fig. 8 that the Z coil will meet the solenoid in NMR performance and, in addition, for the Z coil at the same time heating effects are strongly reduced.

In summary, there are two good reasons to apply coils that are characterized by a low $E_1$ field. Firstly, in the Z coil rf heating of dielectrically dispersive and/or conductive samples is strongly reduced and $B_1$ homogeneity is improved. Secondly, although the Z coil as exemplified in the present paper, has a lower rf efficiency than the solenoidal coils for nonlossy samples, it breaks even with the rf efficiency of the solenoid for lossy samples. This is particularly true for the $^1H$ frequency channel. Taken these two features, rf efficiency and low $E_1$ in conjuction with high $B_1$ homogeneity for lossy samples, the Z coil outperforms the solenoidal coil. Knowing that heating of samples may ruin the NMR experiment, we found that our coil is well suited for HR-MAS applications with biological samples. Z coils are compatible with the existing double or triple resonance circuits in Bruker MAS probes. They represent an alternative to solenoidal coils because they reduce the thermal load on sensitive samples with high dielectric dispersion or electric conductivity resulting from salt content as in biomembrane samples.

## Acknowledgments

We want to express our gratitude to Gerhard Althoff for his assistance in the NMR experiments and to Jesus Raya for instrumental support in Strasbourg. BD is grateful to Irina Munteanu from CST Darmstadt for her help in MWS and to Alexander Krahn for motivating discussions on rf techniques.

## Appendix A. Supplementary data

Supplementary data associated with this article can be found, in the online version, at doi:10.1016/j.jmr.2007.02.018.

## References

[1] P.L. Gor'kov, E. Chekmenev, C. Li, M. Cotten, J.J. Buffy, N.J. Traaseth, G. Veglia, W.W. Brey, Using low-E resonators to reduce RF heating in biological samples for static solid-state NMR up to 900 MHz, J. Magn. Reson. 185 (2007) 77–93.
[2] C. Li, Y. Mo, J. Hu, E. Chekmenev, C. Tian, F. Gao, R. Fu, P. Gor'kov, W. Brey, T. Cross, Analysis of RF heating and sample stability in aligned static solid-state NMR spectroscopy, J. Magn. Reson. 180 (2006) 51–57.
[3] J. Stringer, C. Bronnimann, C. Mullen, D. Zhou, S. Stellfox, Y. Li, E. Williams, C. Rienstra, Reduction of RF-induced sample heating with a scroll coil resonator structure for solid-state NMR probes, J. Magn. Reson. 173 (2005) 40–48.
[4] S. Dvinskikh, V. Castro, D. Sandstrom, Heating caused by radiofrequency irradiation and sample rotation in $^{13}C$ magic angle spinning NMR studies of lipid membranes, Magn. Reson. Chem. 42 (2004) 875–881.
[5] D. Hoult, P. Lauterbur, The sensitivity of the Zeugmatographic experiment involving human samples, J. Magn. Reson. 34 (1979) 425–433.
[6] D. Gadian, F. Robinson, Radiofrequency losses in NMR experiments on electrically conducting samples, J. Magn. Reson. 34 (1979) 449–455.
[7] T. Kotnik, D. Miklavčič, Theoretical evaluation of the distributed power dissipation in biological cells exposed to electric fields, Bioelectromagnetics 21 (2000) 385–394.
[8] M. Simeonova, J. Gimsa, The influence of the molecular structure of lipid membranes on the electric field distribution and energy absorption, Bioelectromagnetics 27 (2006) 652–666.
[9] T. Horiuchi, M. Takahashi, J. Kikuchi, H. Yokoyama, H. Maeda, Effect of dielectric properties of solvents on the quality factor for a beyond 900 MHz cryogenic probe model, J. Magn. Reson. 174 (2005) 34–42.
[10] F. Engelke, Electromagnetic wave compression and radio frequency homogeneity in NMR solenoidal coils: computational approach, Concepts Magn. Reson. B 15 (2002) 129–155.
[11] J. Jackson, Classical Electrodynamics, 3rd ed., Wiley, New York, 1999.
[12] S. Idziak, U. Haeberlen, Design and construction of a high homogeneity RF coil for solid-state multiple-pulse NMR, J. Magn. Reson. 50 (1982) 281–288.
[13] A. Privalov, S. Dvinskikh, H. Vieth, Coil design for large-volume high-B1 homogeneity for solid-state NMR applications, J. Magn. Reson. A 123 (1996) 157–160.
[14] S. Grant, L. Murphy, R. Magin, G. Friedman, Analysis of multilayer radio frequency microcoils for nuclear magnetic resonance spectroscopy, IEEE Trans. Magn. 37 (4) (2001) 2989–2998.
[15] A. Van Geet, Calibration of the methanol and glycol nuclear magnetic resonance thermometers with a static thermistor probe, Anal. Chem. 40 (14) (1968) 2227.
[16] W. Sikorski, A. Sanders, H. Reich, Tris(trimethylsilyl)methane as an internal $^{13}C$ NMR chemical shift thermometer, Magn. Reson. Chem. 36 (1998) S118–S124.
[17] A. Bielecki, D.P. Burum, Temperature dependence of $^{207}Pb$ MAS spectra of solid lead nitrate. An accurate, sensitive thermometer for variable-temperature MAS, J. Magn. Reson. 116 (1995) 215.

[18] N. Lancelot, K. Elbayed, A. Bianco, M. Piotto, Measurement of scaled residual dipolar couplings in proteins using variable-angle sample spinning, J. Biomol. NMR 29 (2004) 259–269.
[19] N. Lancelot, K. Elbayed, M. Piotto, Applications of variable-angle sample spinning experiments to the measurement of scaled residual dipolar couplings and $^{15}N$ CSA in soluble proteins, J. Biomol. NMR 33 (2005) 2–26.
[20] C. Faure, L. Bonakdar, E. Dufourc, Determination of DMPC hydration in the L alpha and L beta phases by $^{2}H$ solid state NMR of $D_2O$, FEBS Lett. 405 (1997) 263–266.
[21] G. Zandomeneghi, Variable-angle spinning NMR techniques for the study of lipid bilayers and bilayer associated peptides, Thesis, ETH Zürich, 2003.
[22] G. Raffard, S. Steinbruckner, A. Arnold, J. Davis, E. Dufourc, Temperature-composition diagram of dimyristoylphosphatidylcholinedicaproyl-phosphatidyl-choline 'bicelles' self-orienting in the magnetic field. A solid-state $^{2}H$ and $^{31}P$ study, Langmuir 16 (2000).
[23] H. Zeiger, B. Dillmann, Hochfrequenz-Spulenanordnung für Messungen mit magnetischer Resonanz und Probenkopf zur Aufnahme von Resonanzsignalen unter Verwendung einer derartigen Hochfrequenz-Spulenanordnung. German Patent DE 10 2005 024 773 B3, 2006.
[24] H. Zeiger, B. Dillmann, Test head for NMR spectrometer, US Patent 7,106,061 B2, 2006.
[25] W. Piasecki, W. Froncisz, Field distributions in loop-gap resonators, Meas. Sci. Technol. 4 (1993) 1363–1369.
[26] M. Alecci, I. Nicholson, D. Lurie, A Novel multiple-tuned radiofrequency loop-gap resonator for use in PEDRI, J. Magn. Reson. B 110 (1996) 82–86.
[27] F. Doty, J. Kulkarni, C. Turner, G. Entzminger, A. Bielecki, Using a crosscoil to reduce RF heating by an order of magnitude in triple-resonance multinuclear MAS at high fields, J. Magn. Reson. 182 (2006) 239–253.
[28] T. Weiland, A Discretization method for the solution of Maxwell equations for six-component fields, AEÜ 31 (1977) 116–120.
[29] M. Clemens, T. Weiland, Discrete electromagnetism with the finite integration technique, Progr. Electromag. Res. 32 (2001) 65–87.
[30] L. Shizhe, Q. Yang, M. Smith, RF coil optimization: evaluation of B1 field homogeneity using field histograms and finite element calculations, Mag. Reson. Imaging 12 (1994) 1079–1087.
[31] H. Torrey, Transient nutations in nuclear magnetic resonance, J. Appl. Phys. 23 (1952) 68–77.
[32] K. Elbayed, B. Dillmann, J. Raya, M. Piotto, F. Engelke, Field modulation effects induced by sample spinning: application to high-resolution magic angle spinning, J. Magn. Reson. 174 (2005) 2–26.
[33] L. Maier, J. Slater, Field strength measurement in resonant cavities, J. Appl. Phys. 23 (1952) 68–77.
[34] E. Paulson, R. Martin, K. Zilm, Cross polarization, radio frequency field homogeneity, and circuit balancing in high-field solid-state NMR probes, J. Magn. Reson. 171 (2004) 314–323.
[35] M. Leifer, RF solenoid with extended equiripple field probe, J. Magn. Reson. A 105 (1993) 1–6.
[36] A. De Angelis, A. Nevzorov, S. Park, S. Howell, A. Mrse, S. Opella, High resolution NMR spectroscopy of membrane proteins in aligned bicelles, J. Am. Chem. Soc. 126 (47) (2004) 15340–15341.
[37] I. Marcotte, M. Auger, Bicelles as model membranes for solid and solution-state NMR studies of membrane peptides and proteins, Concepts Magn. Reson. A 24 (2005) 17–37.
[38] B. Bechinger, J. Seelig, Conformational changes of the phosphatidylcholine headgroup due to membrane dehydration. A $^{2}H$-NMR study, Chem. Phys. Lipids 58 (1991) 1–5.
[39] B. Langer, I. Schnell, H.W. Spiess, A.-R. Grimmer, Temperature calibration under ultrafast MAS conditions, J. Magn. Reson. 138 (1999) 182.
[40] A. Kelly, H. Ou, R. Withers, V. Doetsch, Low-conductivity buffers for high-sensitivity NMR measurements, J. Am. Chem. Soc. 124 (2002) 12013–12019.